Effect of annealing temperature on local distortion of $La_{0.67}Ca_{0.33}MnO_3$ thin films

D. Cao and F. Bridges
Department of Physics, University of California–Santa Cruz, Santa Cruz, California 95064

D. C. Worledge
Department of Applied Physics, Stanford University, Stanford, California 94305-4090

C. H. Booth
Los Alamos National Laboratory, Los Alamos, New Mexico 87545

T. Geballe
Department of Applied Physics, Stanford University, Stanford, California 94305-4090
(Received 30 July 1999; revised manuscript received 6 December 1999)

Mn *K*-edge fluorescence data are presented for thin-film samples (3000 Å) of colossal magnetoresistive (CMR) $La_{0.67}Ca_{0.33}MnO_3$: as deposited, and post annealed at 1000 and 1200 K. The local distortion is analyzed in terms of three contributions: static, phonon, and an extra, temperature-dependent, polaron term. The polaron distortion is very small for the as-deposited sample and increases with the annealing temperature. In contrast, the static distortion in the samples decreases with the annealing temperature. Although the local structure of the as-deposited sample shows very little temperature dependence, the change in resistivity with temperature is the largest of these three thin-film samples. The as-deposited sample also has the highest magnetoresistance, which indicates some other mechanism may also contribute to the transport properties of CMR samples. We also discuss the relationship between local distortion and the magnetization of the sample.

I. INTRODUCTION

The double exchange (DE) mechanism[1–3] was originally considered to be the main interaction contributing to the colossal magnetoresistance (CMR). In the DE model, if the spins of two neighboring Mn ions are aligned, then an electron will require less energy to hop from one Mn site to another. Consequently, at low temperature, the lattice will have ferromagnetic (FM) order such that the total system (both local and itinerant subsystems) has the lowest energy. Although the DE model can explain many properties of CMR materials, the magnitude of the MR calculated from the DE model is much smaller than the actual measured MR.[4] Millis, Littlewood, and Shraiman suggested that local Jahn-Teller distortions also play an important role in CMR materials, and are needed to explain the large magnitude of the MR (Ref. 4) in these materials.

Both x-ray-absorption fine-structure (XAFS) (Refs. 5, and 6) and pair-distribution function (PDF) analysis of neutron-diffraction data[7,8] have been done to study the local structure of the CMR materials and an important relationship between the local distortions and magnetism in these materials has been found.[5,6] These experiments investigate the local structure of thin films of $La_{0.67}Ca_{0.33}MnO_3$ (LCMO) to understand more about this relationship.

Recent experiments show that the non-fully annealed thin-film samples are oxygen deficient;[9,10] the Curie temperature T_C, the saturated magnetization M_0, and the resistivity peak temperature T_{MI} of the samples increase with increasing the oxygen stoichiometry, while the resistivity of the samples decreases.[9–12] For the fully annealed thin-film sample, T_C and T_{MI} are almost the same as those of the bulk material. It is not yet clear what mechanisms are responsible for suppressing T_C, M_0, and T_{MI} in the other samples. Our experiments on transport and magnetization measurements show similar annealing effects with significant changes in the resistivity and the magnetization. They also show that a huge MR occurs for the films, especially for the as-deposited sample at low temperature.

XAFS experiments on these thin-film samples allow us to observe the local structure around the Mn sites, primarily the local distortion of the Mn-O bonds. This paper focuses on the *changes* in the local structure of CMR thin films that are induced by annealing at different temperatures. These results may also help us to better understand how annealing modifies other sample properties.

Diffraction studies of $LaMnO_3$ and $CaMnO_3$ have been carried out by several groups.[13–15] They show that there are three groups of Mn-O bonds in $LaMnO_3$ with different lengths: 1.91, 1.97, and 2.17 Å,[14] while in $CaMnO_3$ all bond lengths are nearly the same at 1.90 Å (Ref. 15) (variation is within 0.01 Å). Our previous work has compared our XAFS data with the diffraction results, and found that the local structure around the Mn site in LCMO CMR samples is very similar to the average structure determined by the diffraction data. More comparison details are shown in Ref. 6.

In Sec. II, we provide a brief description of the samples and some experimental details. We present the magnetization and transport property data in Sec. III and our XAFS results in Sec. IV. The conclusions are given in Sec. V.

II. SAMPLES AND EXPERIMENTS

The $La_{0.67}Ca_{0.33}MnO_3$ thin-film samples were deposited on $SrTiO_3$ substrates using pulsed laser deposition; each film

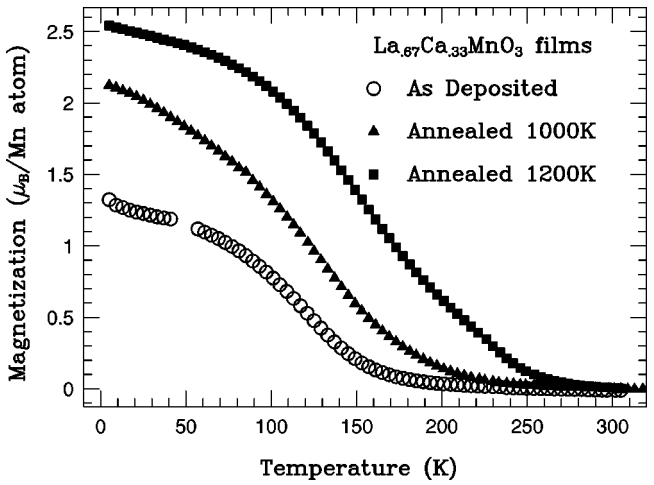

FIG. 1. A plot of magnetization vs temperature for $La_{0.67}Ca_{0.33}MnO_3$ thin-film samples, with an applied field of $H = 5000$ Oe.

is 3000 Å thick. See Ref. 10 for additional details. The samples we chose for the XAFS studies were: as-deposited at 750 K, annealed at 1000 K, and annealed at 1200 K. The annealed samples were held at their respective temperatures for 10 h in flowing oxygen, and were heated and cooled at 2 K per minute.

The XAFS experiments were done on beamline 10-2 at SSRL using Si⟨220⟩ monochromator crystals and a 13-element Ge detector to collect Mn K_α fluorescence data. The thin-film samples were aligned at $\sim 55.0°$ with respect to the x-ray beam to make x, y and z axes equivalent, and thus correspond to a powder. This angle comes from the polarization dependence of the photoelectric effect.[16] For each sample, we made four sweeps at each temperature; for two of these sweeps, we rotated the sample by 1.5° in order to determine the position of glitches, which must be removed.

III. MAGNETIZATION AND RESISTIVITY

The magnetization vs temperature data for these thin-film samples are shown in Fig. 1. All samples have broad ferromagnetic-to-paramagnetic phase transitions and T_C increases with the annealing temperature. From these measurements, we extract T_C for these samples (see Table I).

The saturated magnetization of the samples increases with annealing temperature. This indicates that at higher annealing temperature, a larger fraction of the sample becomes ferromagnetic in the FM phase at low temperature. Our previous experiments show that the 30% Ca-doped LCMO powder sample has a Curie temperature of ~ 260 K,[17] which is very close to the T_C of the fully annealed thin-film sample.

Figure 2 is a plot of $\ln_e$ of the resistivity vs temperature for all three samples. We show both the data in zero field and at 5.5 T. The resistivity decreases with annealing temperature. At zero field, a large peak is present for the 1000-K annealed sample; the resistivity decreases and the peak moves to higher temperature for the 1200-K annealed sample. There is no metal-to-insulator phase transition for the as-deposited sample; this sample also shows a very large resistivity at low temperature. When the external magnetic field is raised to 5.5 T, the resistivity drops dramatically with magnetic field for the 1000 and 1200 K annealed samples at temperatures near the resistivity peak, and the resistivity peaks move to higher temperature. For the as-deposited sample, the biggest change in MR occurs at the lowest measuring temperature (70 K). It should also be noted that the peak in resistivity is very close to T_C for the 1200-K annealed sample, but well below T_C (over 10 K difference) for the 1000-K annealed sample.

TABLE I. The Curie temperature for each thin-film sample.

Sample	As-deposited	Annealed 1000 K	Annealed 1200 K
T_C(K)	164(5)	202(5)	257(5)

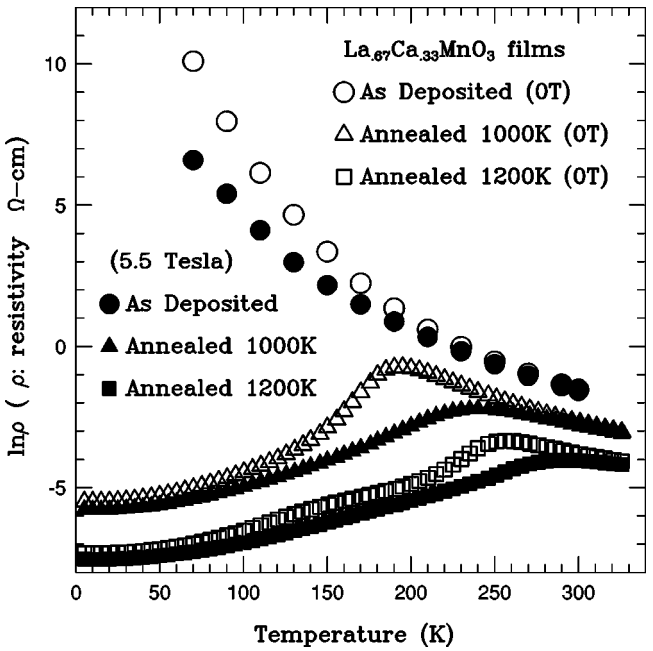

FIG. 2. This plot shows the resistivity data (ln scale) for three thin-film samples, with and without magnetic field. The open symbol corresponds to data without field and the solid symbol corresponds to the data with a field of 5.5 T. There is a double peak structure for the 1200 K annealed sample around 150 K, which is just visible in this figure.

Figure 3 shows CMR% (expressed as a percentage) vs temperature data for these samples on a $\ln_e$ scale. Here, we define CMR% to be

$$\mathrm{CMR\%} = 100 \cdot (R_0 - R_H)/R_H ,$$

where R_0 is the resistivity without magnetic field and R_H is the resistivity with a 5.5-T field.

The magnetoresistance for these thin films is very large compared to that of the corresponding powder samples.[6] This is especially true for the as-deposited sample at low temperature—the change of magnetoresistance at 70 K is about 3200%. The maximum CMR% is about 1000% for the 1000-K sample and about 250% for the 1200-K sample.

There is a double peak structure for the 1200-K annealed sample clearly visible in Fig. 3. As mentioned earlier, our thin-film samples are deposited on $SrTiO_3$(STO) substrates. When the sample is deposited on STO, some Sr diffuses into the first few hundred Å of the film and changes the stoichi-

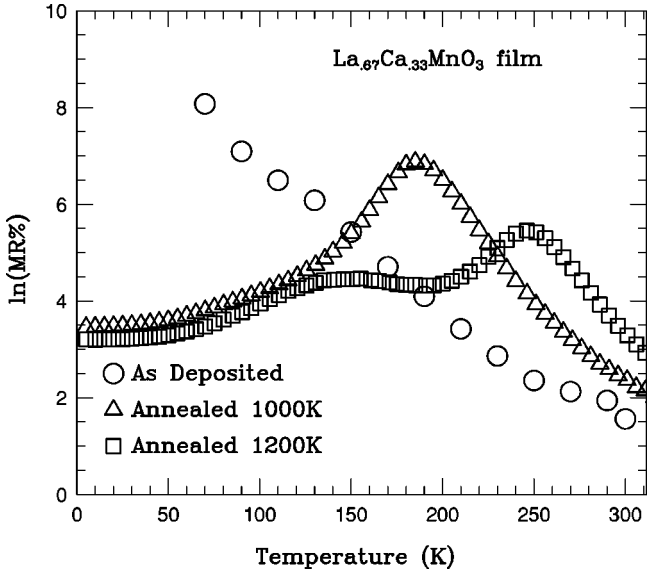

FIG. 3. A plot of CMR% (ln scale) vs temperature for $La_{0.67}Ca_{0.33}MnO_3$ thin-film samples in a field of 5.5 T. The double peak structure for the 1200-K annealed sample is obvious in this plot.

ometry of that layer. This Sr diffusion could produce a resistance peak at a lower temperature and may be responsible for this extra peak. We chose to use STO substrates instead of $LaAlO_3$ (LAO) substrates, which have no diffusion problem, because the large La L_I-edge XAFS from the substrate would interfere with our Mn K-edge XAFS data. Our XAFS data are sensitive to this Sr diffusion layer only if we focus on the further neighbors such as Mn-La, Mn-Ca, and Mn-Sr. The Mn-O bond distance does not change much between Ca and Sr substitution. Consequently, for the Mn-O pair distribution function which is the focus of this paper, we are not very sensitive to Sr in the lower 10% of the film.

IV. XAFS DATA ANALYSIS AND DISCUSSION

We collected all Mn K-edge data in fluorescence mode. First the pre-edge absorption (absorptions from other edges) was removed using the Victoreen formula. Next we extract $k\chi(k)$ where the photoelectron wave vector k is obtained from $k=\sqrt{2m_e(E-E_0)/\hbar^2}$ and the XAFS function $\chi(k)$ is defined as $\chi(k)=\mu(k)/\mu_0(k)-1$. We fit a seven-knot spline to $\mu(k)$ (the K-edge absorption data above the edge) to obtain the background function $\mu_0(k)$ (embedded atom function). An example of such data is shown in Fig. 4. Next we obtain the r-space data from the Fourier transform (FT) of $k\chi(k)$; fits to the data were carried out in r space.[18] Some details of these fits are shown later in this paper. See Refs. 5, 6, and 19 for additional details.

In Fig. 5, we show the Mn K-edge Fourier transformed (FT) r-space data for all three thin-film samples. In this figure, the position of each peak corresponds to an atom pair shifted by a well understood phase shift Δr; for example, the first peak corresponds to the Mn-O pairs and the second peak, which is near 3 Å, corresponds to the Mn-La (Mn-Ca) pairs. The width σ of the pair distribution function is a measure of the local distortions in a shell of neighboring atoms. In XAFS, a large σ leads to a decrease in the amplitude of

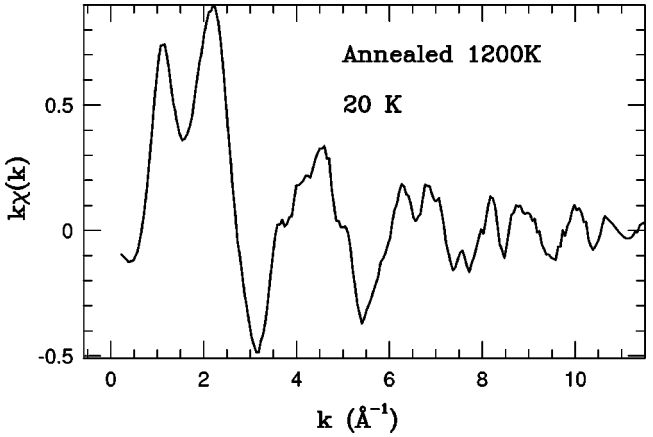

FIG. 4. A plot of the k-space data for the 1200-K annealed sample at 20 K to show the quality of the data. Although there is some noise in the data, the quality is good up to 11 $Å^{-1}$.

the r-space peak. We obtain some results from these data without having to resort to curve fitting. First, the amplitude of the Mn-O peak (the first peak) decreases with increasing temperature. That means there are increasing distortions in each sample with increasing temperature. Second, for the higher annealing temperature, the amplitude at low-temperature increases and the change of the amplitude with temperature for the Mn-O peak is larger than that for the other samples. The amount of distortion removed at low tem-

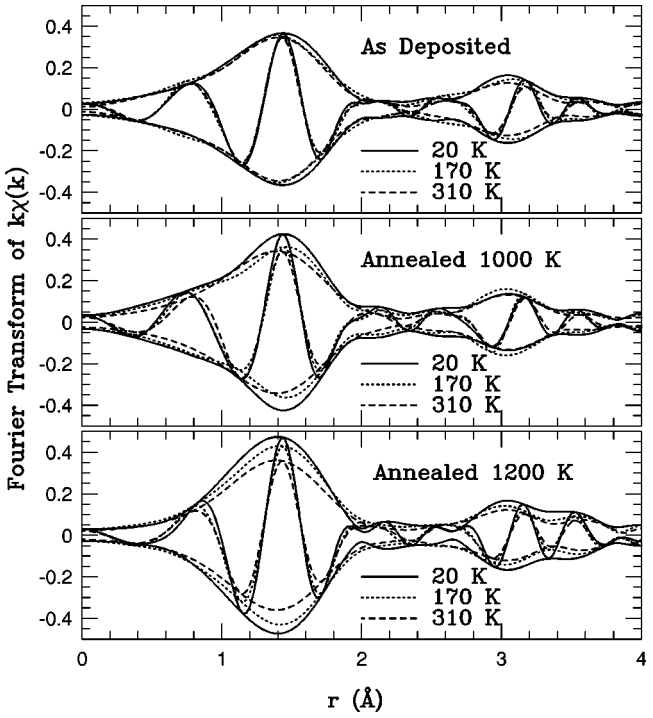

FIG. 5. A comparison of the change in the FT, r-space data with temperature for the $La_{0.67}Ca_{0.33}MnO_3$ thin-film samples with different annealing temperatures. Top: 750-K anneal (as deposited), middle: 1000-K anneal, bottom: 1200-K anneal. FT range is 3.3-10.5 $Å^{-1}$, with 0.3-$Å^{-1}$ Gaussian broadening. The curve inside the envelope, with a higher frequency, is the real part of the FT (FT_R). The envelope is defined as: $\pm\sqrt{FT_R^2+FT_I^2}$ where FT_I is the imaginary part of the FT.

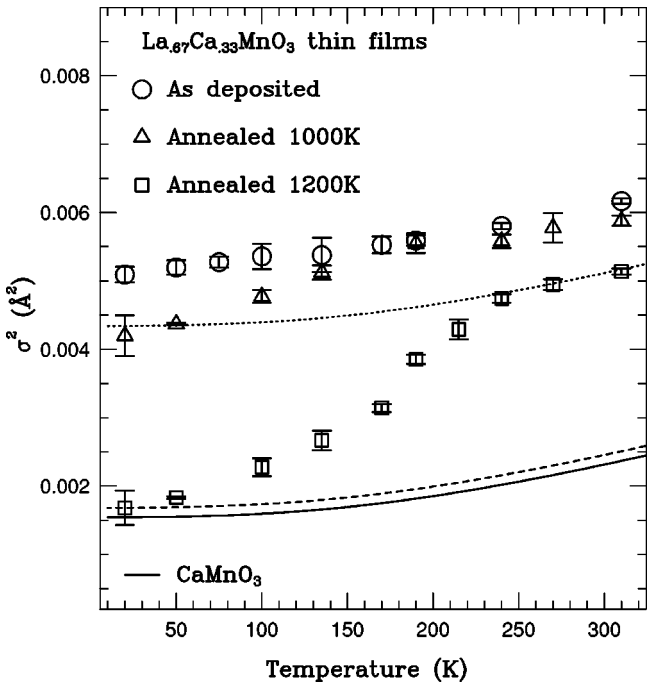

FIG. 6. A plot of σ^2 vs temperature for the as-deposited, 1000-K, and 1200-K annealed $La_{0.67}Ca_{0.33}MnO_3$ thin-film samples. (Here σ is the pair distribution width of the Mn-O peak.) The solid line is the thermal contribution σ_T^2 from $CaMnO_3$,[5,6] the dashed line corresponds to $\sigma_T^2+\sigma_{static}^2$, and the dotted line is $\sigma_T^2+\sigma_{static}^2+\sigma_{FP}^2$ for the annealed 1200-K sample (see text).

perature is smaller for the 1000-K annealed sample, while most of the distortion in the as-deposited sample is still present at $T=20$ K. The amplitude of the *r*-space data at high temperature (310 K) is almost the same for all three samples; this suggests that the amount of distortion at high temperatures does not change very much with the annealing temperature; however, it is still clearly less than the local distortion observed previously in $LaMnO_3$ at 300 K.[5,6]

Our *r*-space data were fit using a Gaussian pair distribution function for the Mn-O, Mn-Ca/La and Mn-Mn shells. The pair distribution width $\sigma(T)$ (for Mn-O) was determined from these detailed fits to the data, which were carried out using FEFF6 theoretical functions[20] (see Fig. 6). In the fit, S_0^2N was fixed at 4.3, where N is the number of nearest neighbors (six O neighbors), and S_0^2 is an amplitude reduction factor. $k\chi(k)$ arrives from single-electron process and is normalized to the step height; S_0^2 corrects for the fact that the measured step height also includes multielectron process. There is an absolute uncertainty in S_0^2 of roughly 10%, however small changes in S_0^2 move all the curves up or down in Fig. 6 and do not change the shape or relative position.

The values of σ^2 obtained from the fits provide a measure of the distortion of the Mn-O bond. Different contributions to the broadening add in quadrature and hence σ^2 has the general form

$$\sigma^2=\sigma_{static}^2+\sigma_{phonons}^2+\sigma_{other\ \ mechanisms}^2.$$

At low temperature, σ^2 is dominated by zero-point motion and some static distortions. For all the manganites, the smallest value for σ is about 0.04 Å; consequently, small variations in bond lengths, such as occurring for $CaMnO_3$ are not directly observed in σ. It is surprising that the net distortion of the substituted CMR samples is about as small as that observed for the more ordered $CaMnO_3$ structure at 20 K.

For each temperature four traces are analyzed and averaged. The relative errors shown in Fig. 6 are the root-mean-square (rms) variation of the fit result at each temperature. For the as-deposited sample, σ^2 has a very small change with decreasing temperature; there is a larger change for the 1000-K annealed sample, and an even larger temperature dependence for the 1200-K annealed sample. We also find in Fig. 6 that, at 320 K, σ^2 increases as the annealing temperature is lowered. This indicates that some of the static defects in the as-deposited sample can be removed during the annealing process.

The solid line in Fig. 6 corresponds to the data for the Mn-O bond in $CaMnO_3$, which has a high Debye temperature (950 K); σ^2 for this sample will be denoted σ_T^2. (The $CaMnO_3$ data we use in this figure are obtained from a powder sample.[6] There might be a difference up to 10% between powder samples and thin-film samples since they are in different form and this difference may change the effective value of S_0^2 for the fit process.)

The difference between σ_{data}^2 and σ_T^2 at low temperature is due to a static distortion σ_{static}^2, which is defined as

$$\sigma_{static}^2=\sigma_{data}^2(20\ \mathrm{K})-\sigma_T^2(20\ \mathrm{K}).$$

To estimate this quantity, we shift the solid line vertically until it fits the low-temperature data for the 1200-K annealed sample. This yields the dashed line in Fig. 6, which is defined to be $\sigma_T^2+\sigma_{static}^2$. Although σ_{static}^2 is almost zero for the 1200-K annealed sample, it is large for the other samples. We include it here for the 1200-K annealed sample to clarify its definition. The contribution to σ_{data}^2 above the dashed line is attributed to a polaron distortion, where the full (maximum) polaron distortion σ_{FP}^2 is defined by

$$\sigma_{FP}^2=\sigma_{data}^2(300\ \mathrm{K})-\sigma_T^2(300\ \mathrm{K})-\sigma_{static}^2.$$

We have found in previous work[5,6] that a useful parameter is the distortion removed as T drops below T_C, $\Delta\sigma^2$, which we define below. First, the σ_T^2 curve is shifted vertically (by an amount $\sigma_{FP}^2+\sigma_{static}^2$) such that it fits the high-temperature data. This yields the dotted line shown in Fig. 6 which is $\sigma_T^2+\sigma_{static}^2+\sigma_{FP}^2$. This dotted line represents the expected Debye behavior plus static distortion if no polaron distortion were removed upon cooling. We define $\Delta\sigma^2$ as the difference between the dotted line and the data:

$$\Delta\sigma^2=\sigma_T^2+\sigma_{FP}^2+\sigma_{static}^2-\sigma_{data}^2.$$

A similar analysis is carried out for the as-deposited sample and the 1000-K annealed sample (corresponding curves for $\sigma_T^2+\sigma_{static}^2$ and $\sigma_T^2+\sigma_{static}^2+\sigma_{FP}^2$ are not shown in Fig. 6). It is also important to point out that the difference between σ^2 for the 1200-K annealed sample and that of $CaMnO_3$ at 20 K is very small, which suggests that the Mn-O local structure of the fully annealed sample can be as ordered as that of $CaMnO_3$ even though it is a doped sample.

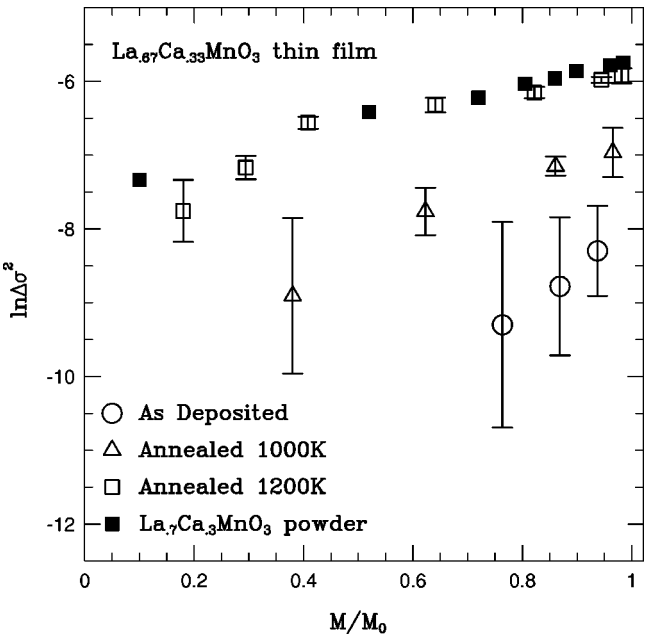

FIG. 7. A plot of $\ln\Delta\sigma^2$ vs M/M_0 is presented for the as-deposited, 1000-K, and 1200-K annealed $La_{0.67}Ca_{0.33}MnO_3$ thin-film samples, as well as a $La_{0.70}Ca_{0.30}MnO_3$ powder sample. M is the measured magnetization and M_0 is the saturated magnetization; M/M_0 is the relative magnetization.

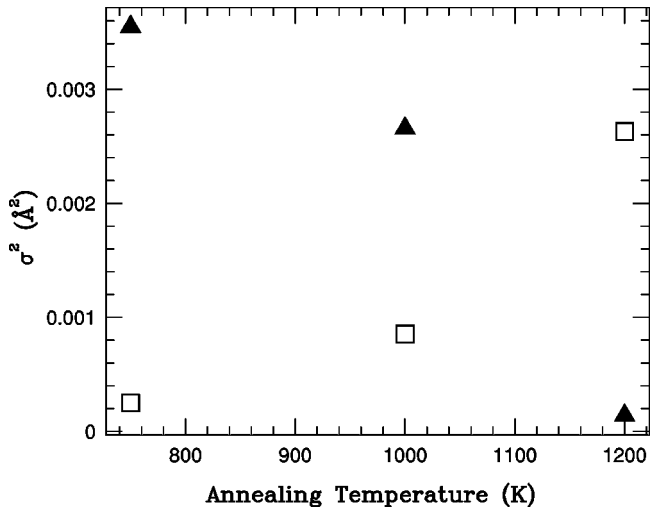

FIG. 8. Static and polaron distortion vs annealing temperature for all three thin-film samples. The solid triangle symbol represents the static distortion, σ^2_{static}; the open square symbol represents the full-polaron distortion σ^2_{FP}.

The same result was obtained for $La_{1-x}Ca_xMnO_3$ CMR powder samples ($x=0.2\sim0.5$) from our previous experiments.[5,6] The reason for this phenomena for the thin films can be explained as follows: first, the high-temperature annealing process appears to remove most of the static defects such as dislocations and vacancies; second, at very low temperatures, there is almost no difference between the two types of Mn sites in the DE model, the electron moves rapidly from one site to another on a time scale fast compared to the appropriate phonon frequency. Consequently, Jahn-Teller distortions do not have time to form.

For the as-deposited sample, the large CMR% occurs when there is a large value for σ^2 at low temperature; this suggests that the distortion in the sample may, in part, be the origin of the unusually large magnetoresistance in thin-film samples. We have recently observed similar results in our study of Ti- and Ga-doped LCMO powder samples.[21]

In Fig. 7, we plot $\ln\Delta\sigma^2$ vs M/M_0. Our previous studies of $La_{1-x}Ca_xMnO_3$ powder samples showed that there is a linear relationship between $\ln\Delta\sigma^2$ and the magnetization,[5,6] which provides evidence that there is a strong connection between the local distortion and magnetism in these materials. The solid squares in Fig. 7 show the linear relationship for a $La_{0.70}Ca_{0.30}MnO_3$ powder sample from our previous work.[5,6] For the thin-film samples, there is a similar connection between local distortion and magnetization. For the 1000- and 1200-K annealed samples, we find a small deviation from a straight line below $M/M_0\sim0.3$. Since the error of the data in this range ($M/M_0<0.3$) is large, it is not clear if this is a real effect or not. The data for the as-deposited sample appear to follow a straight line, but the errors in the difference are too large to draw conclusions. Also, we find that the data for the 1200-K annealed thin-film and the powder sample (both $La_{0.70}Ca_{0.30}MnO_3$) almost overlap each other. This suggests that the local structure of the fully annealed thin film behaves similarly to that of the corresponding bulk sample.

In order to see the effect of annealing temperature on the local distortion more clearly, we plot the distortion contributions σ^2_{static} and σ^2_{FP} as a function of annealing temperature in Fig. 8. This figure shows that the static distortion decreases with annealing temperature, while the polaron contribution increases with annealing temperature. This suggests that part of the static distortions observed in the as-deposited sample become dynamic, polaronlike, distortions after annealing, for $T>T_C$.

It should be noted that although the magnetization only drops by roughly 50% for the as-deposited sample, the σ^2_{FP} contribution becomes much smaller (of order 5%). Consequently, there must be statically distorted regions in the as-deposited sample that are also ferromagnetic. The reduction of the saturated magnetization can arise in several ways. First, because of the inhomogeneous material, small regions may be antiferromagnetic (AF). Second, it has been suggested that the crystal field, particularly in regimes where the inhomogeneity causes a local reduction of the tolerance factor, can result in a low spin Mn($^4t_{2g}$) configuration with a local 50% decrease in Mn moment.[22] Third, the spins in a small domain may not be exactly parallel. However, to explain the entire decrease in saturated magnetization would require very large canting angles. Fourth, the magnetization vectors of each domain may not be aligned. The number of domain walls may be important for calculating the resistivity. However, for domains large compared to a unit cell, slightly canted spins within a domain or a lack of alignment of the magnetization of various domains would not lead to a significant decrease in the polaron contribution to the broadening in XAFS. Consequently, the presence of static distortions but essentially no polaronlike contributions in the as-deposited material indicate both a significant fraction of AF material, and the presence of some low spin Mn sites, possibly induced by the disorder (interstitials, vacancies, inhomogeneous Ca concentrations, etc.). This disorder must pin

the local distortions which would also suppress the electron hopping frequency, thereby reducing the effectiveness of the DE interaction.

All three thin-film samples were prepared in the same way, except for the annealing temperature. During the annealing process, part of the static defects in the sample such as vacancies and interstitials can be removed. In addition, the annealing process can also change the amount of oxygen in the sample.[9–12] The sample is slightly oxygen deficient before the annealing process, and oxygen is incorporated during annealing. The fully annealed sample (1200 K) is expected to be fully stoichiometric (similar to the corresponding powder sample). It is well documented that samples without sufficient oxygen can have higher resistivities, a lower resistance peak temperature, a lower T_C and a lower saturated magnetization.[9–12] We have the same trends in our experiments.

Compared to the 1200-K annealed sample, the samples annealed at lower temperatures have a large decrease in σ_{FP}^2 and a large increase in resistivity, while the saturated magnetization changes by less than a factor of 2. This suggests that much of the distorted magnetic regions probably do not contribute to the conductivity and that the fraction of conducting material is very low for the as-deposited sample. However, the six orders of magnitude increase in resistivity is much larger than the volume reduction of the regions that still have a polaronlike distortion. Consequently, it is likely that percolation also plays a role for transport in the as-deposited sample. Then the magnetic field may play two roles for this sample; it will decrease the resistivity for the conducting pathways that exist at $B=0$ and may also make some ''marginal'' pathways become conducting.

V. CONCLUSION

From our analysis, we find that the annealing temperature of the thin films affects the local distortion of the materials appreciably. The large change in resistivity and the small change in local structure with temperature for the as-deposited sample suggest that only small regions are contributing to the resistivity and percolation may play a role. We also find that there is still a strong connection between local distortions, resistivity, and magnetism in the fully annealed thin-film materials, which behaves much like a powder sample. For the 1000-K annealed sample, the resistivity and MR peaks are well below T_C. In this case (including the as-deposited sample), the local distortions correlate well with the magnetization, but there is no feature in σ that occurs at the temperature at which the resistivity has a peak.

ACKNOWLEDGMENTS

This work was supported in part by NSF Grant No. DMR9705117. The experiments were performed at SSRL, which is operated by the DOE, Division of Chemical Sciences, and by the NIH, Biomedical Resource Technology Program, Division of Research Resources.

[1] C. Zener, Phys. Rev. **82**, 403 (1951).
[2] P.W. Anderson and H. Hasegawa, Phys. Rev. **100**, 675 (1955).
[3] P.G. de Gennes, Phys. Rev. **118**, 141 (1960).
[4] A.J. Millis, P.B. Littlewood, and B.I. Shraiman, Phys. Rev. Lett. **74**, 5144 (1995).
[5] C.H. Booth, F. Bridges, G.H. Kwei, J.M. Lawrence, A.L. Cornelius, and J.J. Neumeier, Phys. Rev. Lett. **80**, 853 (1998).
[6] C.H. Booth, F. Bridges, G.H. Kwei, J.M. Lawrence, A.L. Cornelius, and J.J. Neumeier, Phys. Rev. B **57**, 10 440 (1998).
[7] S.J.L. Billinge, R.G. DiFrancesco, G.H. Kwei, J.J. Neumeier, and J.D. Thompson, Phys. Rev. Lett. **77**, 715 (1996).
[8] D. Louca, T. Egami, E.L. Brosha, H. Röder, and A.R. Bishop, Phys. Rev. B **56**, R8475 (1997).
[9] D.C. Worledge, G. Jeffrey Snyder, M.R. Beasley, and T.H. Geballe, J. Appl. Phys. **80**, 5158 (1996).
[10] D.C. Worledge, L. Mieville, and T.H. Geballe, J. Appl. Phys. **83**, 5913 (1998).
[11] H.L. Ju, J. Gopalakrishnan, J.L. Peng, Qi Li, G.C. Xiong, T. Venkatesan, and R.L. Greene, Phys. Rev. B **51**, 6143 (1995).
[12] N. Malde, P.S.I.P.N. De Silva, A.K.M. Akther Hossain, L.F. Cohen, K.A. Thomas, J.L. MacManus-Driscoll, N.D. Mathur, and M.G. Blamire, Solid State Commun. **105**, 643 (1998).
[13] P. Norby, I.G. Krogh Andersen, E. Krogh Andersen, and N.H. Andersen, J. Solid State Chem. **119**, 191 (1995).
[14] J.F. Mitchell, D.N. Argyriou, C.D. Potter, D.G. Hinks, J.D. Jorgensen, and S.D. Bader, Phys. Rev. B **54**, 6172 (1996).
[15] K.R. Poeppelmeier, M.E. Leonowicz, J.C. Scanlon, and J.M. Longo, J. Solid State Chem. **45**, 71 (1982).
[16] R.F. Pettifer, C. Brouder, M. Benfatto, C.R. Natoli, C. Hermes, and M.F. Ruiz Lopez, Phys. Rev. B **42**, 37 (1990).
[17] P. Schiffer, A. Ramirez, W. Bao, and S-W. Cheong, Phys. Rev. Lett. **75**, 3336 (1995).
[18] T.M. Hayes and J.B. Boyce, Solid State Phys. **37**, 173 (1982).
[19] J.J. Rehr, C.H. Booth, F. Bridges, and S.I. Zabinsky, Phys. Rev. B **49**, 12 347 (1994).
[20] S.I. Zabinsky, A. Ankudinov, J.J. Rehr, and R.C. Albers, Phys. Rev. B **52**, 2995 (1995).
[21] D. Cao, F. Bridges, A. P. Ramirez, M. Olapinski, M. A. Subramanian, C. H. Booth, and G. Kwei (unpublished).
[22] T. H. Geballe and B. Y. Moyzches (unpublished).